Comput Mech (2010) 46:269–285
DOI 10.1007/s00466-009-0400-9

ORIGINAL PAPER

A method of two-scale thermo-mechanical analysis for porous solids with micro-scale heat transfer

K. Terada · M. Kurumatani · T. Ushida · N. Kikuchi

Received: 9 February 2009 / Accepted: 26 May 2009 / Published online: 12 June 2009

Abstract A two-scale thermo-mechanical model for porous solids is derived and is implemented into a multi-scale multi-physics analysis method. The model is derived based on the mathematical homogenization method and can account for the scale effect of unit cells, which is our particular interest in this paper, on macroscopic thermal behavior and, by extension, on macroscopic deformation due to thermal expansion/contraction. The scale effect is thought to be the result of microscopic heat transfer, the amount of which depends on the micro-scale pore size of porous solids. We first formulate a two-scale model by applying the method of asymptotic expansions for homogenization and, by using a simple numerical model, verify the validity and relevancy of the proposed two-scale model by comparing it with a corresponding single-scale direct analysis with detailed numerical models.

Keywords Porous solids · Thermo-mechanics · Scale effect · Homogenization method · Micro-scale heat transfer

1 Introduction

Many types of materials, including ceramics, concrete, asphalt, soils and rocks, are categorized into porous solids with pores either artificially made for a specific purpose or naturally formed by a physical process. Such materials tend to have very small pores, which may be open and connected, or closed, and are often subjected to thermal or chemical attack at the internal boundaries formed by pores as well as the external boundaries. Because the strength, stiffness and durability of porous solids rely on their mechanical characteristics under certain thermal and chemical conditions, which can be determined by transport phenomena [1], the thermo-mechanical or chemo-mechanical coupling problems are of particular importance. Inevitably, our attention is focussed on the so-called scale effect of the pore size on the characteristics of heat conduction or transfer, mass diffusion and deformation of porous solids possibly accompanied with fluid flow in the pores, as pointed out in the literature [2–4].

Since the direct numerical modeling of an assembly of small pores as a medium for numerical analyses requires considerable computational costs, the introduction of equivalent media with average or effective thermal and poroelastic properties has been common practice. In this context, the approaches based on the mathematical homogenization method [5,6] have attracted attention affinity to numerical methods such as finite element methods (FEM); see [7,8] for relatively early developments to demonstrate the promise and potential of such approaches.

Applications of computational homogenization approaches to thermal or poroelastic problems are too numerous to mention [9–14]. Some of them deal with thermo-mechanical coupling phenomena [15,16]. Although the theoretical and computational aspects of the homogenization approaches seem to be mature, very few serious attempts have been made to realize the aforementioned scale effect on the heat conduction or transfer characteristics of porous solids. In fact, no attention has been paid to the incorporation of the effect with overall deformation behavior. This is partially because formulation in consideration of the scale effect for heat conduction problems is somewhat special [17], with the help of the

K. Terada (✉) · M. Kurumatani · T. Ushida
Department of Civil Engineering, Tohoku University, Aza-Aoba 6-6-06, Aramaki, Aoba-ku, Sendai 980-8579, Japan
e-mail: tei@civil.tohoku.ac.jp

N. Kikuchi
Department of Mechanical Engineering, The University of Michigan, 2350 Hayward, Ann Arbor, MI 48109-2125, USA

method of asymptotic expansions [6], and is not mentioned even in the monograph for the homogenization of porous solids [18].

In this paper, we derive a two-scale thermo-mechanical model for porous solids that can account for the scale effect of unit cells by applying the mathematical homogenization method, and develop a multi-scale multi-physics analysis method for simulating the thermo-mechanical coupled behavior characterized by the proposed model. Since heat is supposed to be transferred from the micro-scale pores in the model, the macroscopic conduction characteristics of porous media are affected by the pore size and, by extension, such a scale effect also appears on the macroscopic deformation due to thermal expansion/contraction. The formulation is inserted in the Japanese monograph by Terada and Kikuchi [17], but has not yet been reported in journal articles.

After the two-scale model is formulated with the method of asymptotic expansions, its validity and relevancy is verified by comparing it with the corresponding single-scale direct analysis with detailed unit cell models. For this numerical verification, we employ a simple but intentioned porous medium model with open and connected pores that are filled with a fluid, since the heat is supposed to be conducted in the filling fluid, which does not flow in this study.

2 Preliminaries to the asymptotic homogenization for thermo-mechanical problem

2.1 Assumptions

We consider a coupled problem of quasi-static deformation with thermal expansion/contraction and transient heat conduction in porous solids. The pores are assumed to be infinitesimally small, and only the sources of micro-scale heterogeneity that governs the overall thermo-mechanical behavior of the media. The pores are also assumed to be periodically arranged so that the periodic microstructure, i.e., the unit cell, with one or two pores can be identified with a representative volume element (RVE) within the framework of the mathematical homogenization [6,17].

We suppose that the pores may be filled with a fluid that does not flow. It is then assumed that the heat is transferred at the pore surfaces from the fluid phase to the solid phase. This means that the macroscopic heat conduction is characterized not only by the micro-scale heat conduction but also the effect of the micro-scale heat transfer. Note here that the fluid is regarded just as a medium that delivers and provides the heat to the solid phase.

It is assumed that the solid phase is a linearly elastic solid and the deformation is infinitesimally small. This assumption may justify the condition in which material properties for heat conduction and transfer in the solid phase are not affected by deformation. That is, the coupling behavior is assumed to be one way form the temperature field of the fluid phase to the deformation of the solid phase due to temperature change, i.e., thermal expansion/contraction.

2.2 Governing equations of the original problems

Let us consider the domain of a porous solid denoted by $\Omega^\epsilon \subset \mathcal{R}^{n_{\rm dim}}$ with a smooth boundary $\partial\Omega^\epsilon$. Here, ϵ indicates the representative size of the unit cell, and $n_{\rm dim}$ (=1, 2, or 3) is a spatial dimension of the problem, $\mathcal{R}$ is the space of real numbers. We assume that the pores, or voids, in the medium are open and connected. Figures 1 and 2, respectively, schematize separate homogenization procedures for an unsteady heat conduction problem with micro-scale heat transfer and a deformation problem with thermal expansion/contraction in the same domain. The upper figures of each show the corresponding original problems before being homogenized, where the sub- or superscript ϵ are attached to the field variables so that they are dependent on the microstructure. In this subsection, we provide the governing equations of the original heat conduction and deformation problems by means of this notational rule.

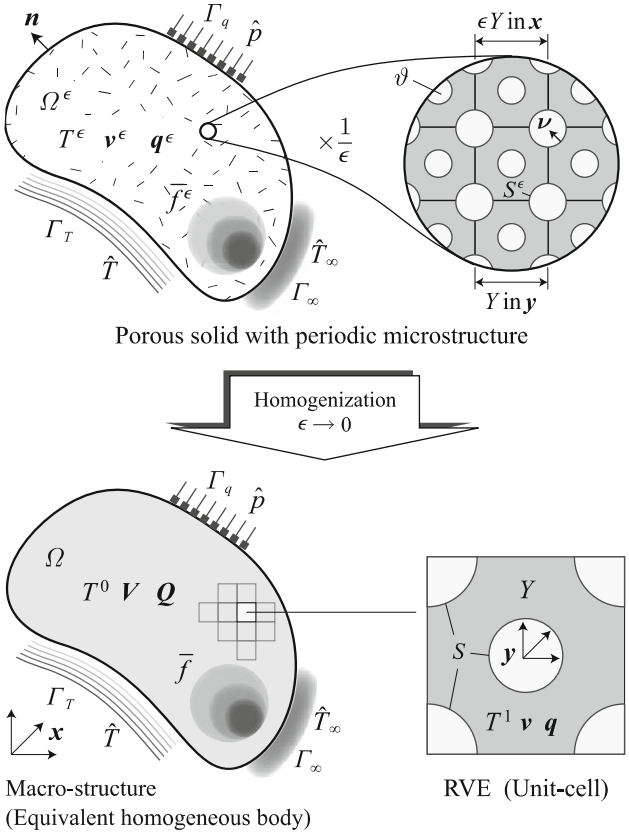

Fig. 1 Homogenization for heat conduction problem

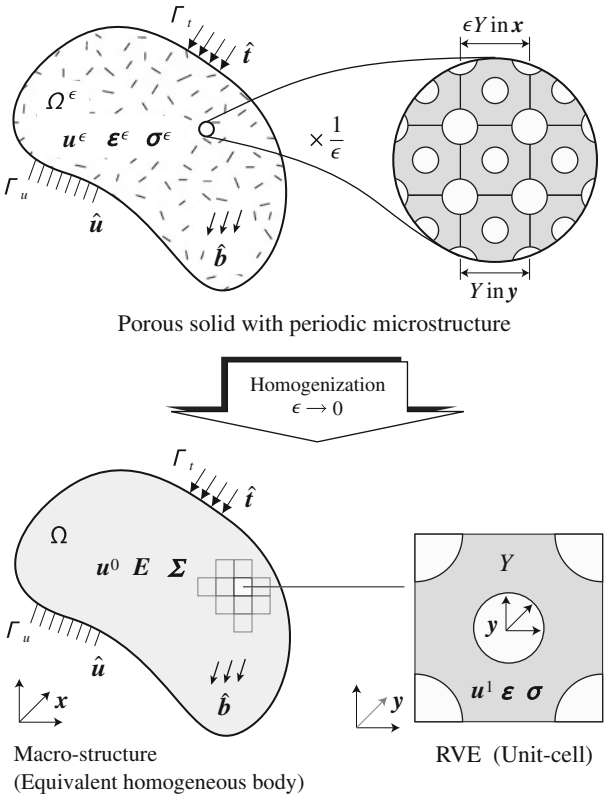

Fig. 2 Homogenization for solid deformation problem

2.2.1 Transient heat conduction problem

The governing equations of the original heat conduction problem for without advection are given at any point $\boldsymbol{x} \in \Omega^\epsilon$ and at any time $t \in [0, \infty)$ as follows:

$$c^\epsilon \rho^\epsilon \dot{T}^\epsilon = -\nabla \cdot \boldsymbol{q}^\epsilon + f^\epsilon \quad \text{in } \Omega^\epsilon \tag{1}$$

$$\boldsymbol{q}^\epsilon = -\boldsymbol{k}^\epsilon \boldsymbol{v}^\epsilon \quad \text{in } \Omega^\epsilon \tag{2}$$

$$\boldsymbol{v}^\epsilon = \nabla T^\epsilon \quad \text{in } \Omega^\epsilon \tag{3}$$

where, with t being the current time, $T = T^\epsilon(\boldsymbol{x}, t)$ is the temperature field, and $\boldsymbol{q}^\epsilon(\boldsymbol{x}, t)$ is the heat flux, which is related to the temperature gradient $\boldsymbol{v}^\epsilon(\boldsymbol{x}, t)$ via the positive definite, second-order heat conduction tensor $\boldsymbol{k}^\epsilon(\boldsymbol{x})$. Here, ∇ is the gradient operator, $(\dot{\bullet}) := \mathrm{D}/\mathrm{Dt}$ is the material time derivative, c^ϵ is the specific heat, ρ^ϵ is the mass density, and f^ϵ is the heat source.

We consider the following three types of boundary conditions on the part of the boundary $\Gamma^\epsilon \subset \partial\Omega^\epsilon$, whose outward unit normal vector is commonly denoted by $\boldsymbol{n}$:

$$T^\epsilon = \hat{T} \quad \text{on } \Gamma_T \tag{4}$$

$$\boldsymbol{q}^\epsilon \cdot \boldsymbol{n} = \hat{p} \quad \text{on } \Gamma_q \tag{5}$$

$$\boldsymbol{q}^\epsilon \cdot \boldsymbol{n} = k_\infty (T^\epsilon - \hat{T}_\infty) \quad \text{on } \Gamma_\infty \tag{6}$$

where $\hat{T}$ is the temperature data specified on the Dirichlet boundary Γ_T and $\hat{p}$ is the heat supplied on the Neumann boundary Γ_q. Also, the heat is supplied from Γ_∞ with the coefficient of heat transfer k_∞ according to the ambient temperature $\hat{T}_\infty$. It is noted that $\Gamma^\epsilon = \Gamma_T \cup \Gamma_q \cup \Gamma_\infty \subset \partial\Omega^\epsilon$ and $\Gamma_T \cap \Gamma_q \cap \Gamma_\infty = \emptyset$. In addition, the heat transfer is allowed on the pore surfaces as

$$\boldsymbol{q}^\epsilon \cdot \boldsymbol{v} = k_S^\epsilon (T^\epsilon - \hat{T}_S) \quad \text{on } S^\epsilon \tag{7}$$

where $S^\epsilon = \partial\Omega^\epsilon \backslash \Gamma^\epsilon$ is the sum of all the pore surfaces, $\boldsymbol{v}$ is its outward unit normal vector, $\hat{T}_S$ is the temperature of the fluid filling the pores, and k_S^ϵ is the coefficient of heat transfer in distinction from k_∞. Although the pores may or may not appear on the external boundary of the overall structure, it is assumed that the heat transfer characteristics can be represented by k_∞, irrespective of its geometrical features.

The corresponding weak form for the solution $T^\epsilon(\boldsymbol{x}, t)$, which is a function of time t with values in an appropriate function set $\mathcal{U}_T$, is given as follows:

$$\begin{aligned} &\int_{\Omega^\epsilon} c^\epsilon \rho^\epsilon \bar{T}^\epsilon \dot{T}^\epsilon \, d\Omega + \int_{\Omega^\epsilon} \nabla \bar{T}^\epsilon \cdot \boldsymbol{k}^\epsilon \nabla T^\epsilon \, d\Omega \\ &\quad + \int_{\Gamma_\infty} k_\infty \bar{T}^\epsilon (T^\epsilon - \hat{T}_\infty) \, d\Gamma + \int_{S^\epsilon} k_S^\epsilon \bar{T}^\epsilon (T^\epsilon - \hat{T}_S) \, d\Gamma \\ &= \int_{\Omega^\epsilon} \bar{T}^\epsilon f^\epsilon \, d\Omega - \int_{\Gamma_q} \bar{T}^\epsilon \hat{p} \, d\Gamma \quad \forall \bar{T}^\epsilon \in \mathcal{V}_T \end{aligned} \tag{8}$$

where $\bar{T}^\epsilon(\boldsymbol{x})$ is a test function selected arbitrarily from its function space $\mathcal{V}_T$. Finally, we provide the following initial condition to complete the transient heat conduction problem:

$$T^\epsilon(\boldsymbol{x}, 0) = T_0(\boldsymbol{x}) \quad \text{in } \Omega^\epsilon \tag{9}$$

Even if the heat conduction problem for the fluid phase has to be solved simultaneously, the formulation here is unchanged. It is also recognized that the heat conduction problem for the fluid phase is exactly the same as that presented here, when the domain Ω^ϵ is applied to the fluid phase.

2.2.2 Deformation problem with thermal expansion/contraction

Assuming that the deformation process is quasi-static, we here provide the governing equation of the equilibrium problem of a linearly elastic porous solid with thermal expansion/contraction with reference to Fig. 2a. The domain of interest Ω^ϵ is the same domain as that of the heat conduction problem.

The equilibrium equation for stress $\boldsymbol{\sigma}^\epsilon(\boldsymbol{x}, t)$, the relationship between strain $\boldsymbol{\varepsilon}^\epsilon(\boldsymbol{x}, t)$ and displacement $\boldsymbol{u}^\epsilon(\boldsymbol{x}, t)$ and

the constitutive equation are respectively given as follows:

$$\nabla \cdot \boldsymbol{\sigma}^\epsilon + \rho^\epsilon \hat{\boldsymbol{b}} = \mathbf{0} \quad \text{in } \Omega^\epsilon \tag{10}$$

$$\boldsymbol{\varepsilon}^\epsilon = \frac{1}{2}\left\{\nabla \boldsymbol{u}^\epsilon + \boldsymbol{u}^\epsilon \nabla\right\} = \nabla^{(\mathrm{s})}\boldsymbol{u}^\epsilon \quad \text{in } \Omega^\epsilon \tag{11}$$

$$\boldsymbol{\sigma}^\epsilon = \boldsymbol{c}^\epsilon : \boldsymbol{\varepsilon}^\epsilon - \theta^\epsilon \boldsymbol{\beta}^\epsilon = \boldsymbol{c}^\epsilon : \left(\boldsymbol{\varepsilon}^\epsilon - \theta^\epsilon \boldsymbol{\alpha}^\epsilon\right) \quad \text{in } \Omega^\epsilon \tag{12}$$

where $\boldsymbol{c}^\epsilon(\boldsymbol{x})$ is the elasticity tensor, $\hat{\boldsymbol{b}}(\boldsymbol{x})$ is the body force per unit mass density, and $\nabla^{(\mathrm{s})}$ the symmetric gradient operator. Here, θ^ϵ is the temperature change form the initial value T_0 in (9); that is, $\theta^\epsilon(\boldsymbol{x}, t) := T^\epsilon(\boldsymbol{x}, t) - T_0(\boldsymbol{x})$. Also, $\boldsymbol{\alpha}^\epsilon$ and $\boldsymbol{\beta}^\epsilon$ are the second order tensor of thermal expansion coefficients and the thermal expansion stress tensor per unit of temperature change, respectively, and are assumed to have positive diagonal components in general. The following two types of boundary conditions are considered on $\Gamma^\epsilon = \Gamma_u \cup \Gamma_t$ with $\Gamma_u \cap \Gamma_t = \emptyset$:

$$\boldsymbol{u}^\epsilon = \hat{\boldsymbol{u}} \quad \text{on } \Gamma_u \tag{13}$$

$$\boldsymbol{\sigma}^\epsilon \boldsymbol{n} = \hat{\boldsymbol{t}} \quad \text{on } \Gamma_t \tag{14}$$

where $\hat{\boldsymbol{u}}$ and $\hat{\boldsymbol{t}}$ are the prescribed displacement and surface traction vectors, respectively.

The weak form equivalent to the above strong form for the deformation problem is given as follows:

$$\int_{\Omega^\epsilon} \nabla \bar{\boldsymbol{u}}^\epsilon : \boldsymbol{\sigma}^\epsilon \, d\Omega = \int_{\Gamma_t} \bar{\boldsymbol{u}}^\epsilon \cdot \hat{\boldsymbol{t}} \, d\Gamma + \int_{\Omega^\epsilon} \bar{\boldsymbol{u}}^\epsilon \cdot \rho^\epsilon \hat{\boldsymbol{b}} \, d\Omega \quad \forall \bar{\boldsymbol{u}}^\epsilon \in \mathcal{V}_u \tag{15}$$

with which $\boldsymbol{u}^\epsilon \in \mathcal{U}_u$ is searched for via the constitutive equation (12). Here, $\mathcal{U}_u$ is a subset of a relevant Sobolev space with equality constraint (13) and $\mathcal{V}_u$ is an appropriate function space of its variation $\bar{\boldsymbol{u}}$.

We assume that the external loadings $\hat{\boldsymbol{b}}(\boldsymbol{x})$ and $\hat{\boldsymbol{t}}(\boldsymbol{x})$ are constant with respect to time. Also, the temperature change in (12), which causes thermal expansion/contraction of the solid, is actually the solution of the heat conduction problem above described. Therefore, in this study, the temperature change in time is only the source of time dependent loading for the solid phase.

3 Two-scale governing equations for thermo-mechanical coupled problem

The two-scale initial-boundary problem is derived by applying the method of asymptotic expansions to the thermo-mechanical coupled problem for porous solids in consideration of the micro-scale heat transfer, which necessarily enables us to take into account the scale effect of microstructures.

3.1 Two-scale setting: micro- and macro-scale

Within the framework of the mathematical homogenization theory [5,6], two distinct scales are introduced to describe the thermal or mechanical behavior of this body. One is a macro-scale denoted by $\boldsymbol{x}$ for the macroscopic domain Ω, in which the heterogeneities are invisible, and the other is a micro-scale which defines the heterogeneities, and is denoted by $\boldsymbol{y}$ for the microscopic domain of the RVE (unit cell) $Y \subset \mathcal{R}^{n_{\mathrm{dim}}}$. These two scales are related to each other as $\boldsymbol{y} = \boldsymbol{x}/\epsilon$, with the parameter ϵ, which is assumed to be very small compared with the macro-scale bounded domain Ω. Note that the microscopic domain Y of the RVE is the sum of the domains of the solid phase Y^ϑ in the RVE and of pores (or voids) ϑ. That is, for later use in the homogenization, we assume

$$Y^\vartheta = Y \backslash \vartheta \quad \text{and} \quad Y = Y^\vartheta \cup \vartheta. \tag{16}$$

The domain of pore ϑ is assumed to be open and connected, and defines a smooth surface S on the micro-scale solid domain Y^ϑ, which does not intersect with the RVE's external boundary ∂Y. At this internal surface S, the heat is transferred in view of (7). Consideration of this effect in the homogenization is the novelty of the present study.

By virtue of this setting, all the field variables introduced in the previous section are identified with reference to the two scales and $\boldsymbol{y}$ takes charge of representing the dependency on the micro-scale heterogeneity. More specifically, we write the temperature, the temperature gradient vector, the heat flux, the displacement vector, the strain tensor and the stress tensor as $T(\boldsymbol{x}, \boldsymbol{y})$, $\boldsymbol{V}(\boldsymbol{x}, \boldsymbol{y})$, $\boldsymbol{q}(\boldsymbol{x}, \boldsymbol{y})$, $\boldsymbol{u}(\boldsymbol{x}, \boldsymbol{y})$, $\boldsymbol{\varepsilon}(\boldsymbol{x}, \boldsymbol{y})$, $\boldsymbol{\sigma}(\boldsymbol{x}, \boldsymbol{y})$, respectively. It is then postulated in the mathematical theory of homogenization that all the variables are assumed to be periodic with respect to the micro-scale $\boldsymbol{y}$; i.e., Y-periodic [5,6].

In what follows, we apply the conventional method of asymptotic expansions [5,6] to separate the governing equations for heat conduction and deformation problems presented in the previous section to derive the corresponding micro- and macroscopic governing equations. The temperature and the displacement fields are first asymptotically expanded with respect to the characteristic size of the unit cell ϵ and are inserted into the original governing equations. Then, we take the limit ($\epsilon \to 0$) to separate the governing equations in micro- and macro-scales; see also [17,18]. To this end, we extensively utilize the following formulae to separate the micro- and macro-scale volume integrals:

$$\lim_{\epsilon \to 0} \int_{\Omega^\epsilon} \varphi^\epsilon(\boldsymbol{x}) d\Omega = \int_{\Omega} \left[\frac{1}{|Y|} \int_{Y} \varphi(\boldsymbol{x}, \boldsymbol{y}) dy \right] dx \tag{17}$$

where $\varphi^\epsilon = \varphi(\boldsymbol{x}, \boldsymbol{y})$ is an arbitrary function in our problems under consideration; see [6].

Before proceeding to formulation, an important assumption must be confirmed for the order of approximation with asymptotic expansions. That is, we have assumed that the unit cell size is infinitesimally small so that only the first order terms of the asymptotic expansions could be taken into account; higher-order terms are neglected. This means that the macroscopic strain and the macroscopic temperature gradient are assumed to be sufficiently small within the RVE. This is the standard setting for the conventional homogenization theory of the first order approximation. It is then guaranteed that we need not consider fluctuations of the temperature field in time, and that a steady-state temperature distribution can be assumed in the RVE domain. Accordingly, a single time scale is enough for the present setting, although multiple time scales have to be introduced along with multiple spatial scales to distinguish between fast and slow phenomena [19,20].

3.2 Two-scale heat conduction problem

Applying the method of asymptotic expansion, we derive the micro- and macroscopic governing equations, which define the two-scale heat conduction problem. Since the material behavior is assumed to be linear, the formulae of homogenized material properties are also formulated.

3.2.1 Method of asymptotic expansions

First, we assume the solution T^ϵ of the original heat conduction problem and its variation $\bar{T}^\epsilon$ can be asymptotically expanded as

$$T^\epsilon(\boldsymbol{x},t)=T^0(\boldsymbol{x},\boldsymbol{y},t)+\epsilon T^1(\boldsymbol{x},\boldsymbol{y},t)+\epsilon^2 T^2(\boldsymbol{x},\boldsymbol{y},t)+\cdots \tag{18}$$

$$\bar{T}^\epsilon(\boldsymbol{x})=\bar{T}^0(\boldsymbol{x},\boldsymbol{y})+\epsilon\bar{T}^1(\boldsymbol{x},\boldsymbol{y})+\epsilon^2\bar{T}^2(\boldsymbol{x},\boldsymbol{y})+\cdots \tag{19}$$

where terms T^i $(i=0,1,\ldots)$ of order ϵ^i are Y-periodic. Since $\boldsymbol{y}=\boldsymbol{x}/\epsilon$, the chain rule can be applied for the differentiation of each term with

$$\left.\frac{\partial}{\partial x_i}\right|_{\Omega^\epsilon}\boldsymbol{e}_i=\left(\left.\frac{\partial}{\partial x_i}\right|_{\Omega}+\frac{1}{\epsilon}\left.\frac{\partial}{\partial y_i}\right|_{Y}\right)\boldsymbol{e}_i=\nabla_x+\frac{1}{\epsilon}\nabla_y \tag{20}$$

Substituting (18) and (19) into (8) and neglecting higher-order terms (higher than or equal to the second order terms with ϵ^2), we have the following weak form:

$$\begin{aligned}
&\int_{\Omega^\epsilon} c^\epsilon\rho^\epsilon\left(\bar{T}^0+\epsilon\bar{T}^1\right)\left(\dot{T}^0+\epsilon\dot{T}^1\right)d\Omega\\
&\quad+\int_{\Omega^\epsilon}\left(\frac{1}{\epsilon}\nabla_y\bar{T}^0+\nabla_x\bar{T}^0+\nabla_y\bar{T}^1+\epsilon\nabla_x\bar{T}^1\right)\\
&\quad\cdot\boldsymbol{k}^\epsilon\left(\frac{1}{\epsilon}\nabla_y T^0+\nabla_x T^0+\nabla_y T^1+\epsilon\nabla_x T^1\right)d\Omega\\
&\quad+\int_{\Gamma_\infty}k_\infty\left(\bar{T}^0+\epsilon\bar{T}^1\right)\left(T^0+\epsilon T^1\right)d\Gamma\\
&\quad+\int_{S^\epsilon}\epsilon k_S\left(\bar{T}^0+\epsilon\bar{T}^1\right)\left(T^0+\epsilon T^1\right)d\Gamma\\
&=\int_{\Omega^\epsilon}\left(\bar{T}^0+\epsilon\bar{T}^1\right)f^\epsilon d\Omega-\int_{\Gamma_q}\left(\bar{T}^0+\epsilon\bar{T}^1\right)\hat{p}d\Gamma\\
&\quad+\int_{\Gamma_\infty}k_\infty\left(\bar{T}^0+\epsilon\bar{T}^1\right)\hat{T}_\infty d\Gamma\\
&\quad+\int_{S^\epsilon}\epsilon k_S\left(\bar{T}^0+\epsilon\bar{T}^1\right)\hat{T}_S d\Gamma
\end{aligned} \tag{21}$$

Here, we have assumed that the coefficient of heat transfer k_S^ϵ on the pore surface S^ϵ depends linearly on the characteristic length ϵ of the unit cell; that is,

$$k_S^\epsilon=\epsilon k_S. \tag{22}$$

This assumption can be accepted by the insight that the area of the pore surface becomes finite when the volume of the unit cell becomes zero in the asymptotic process with $\epsilon\to 0$ in the sequel. This can be explained in a little more detail with reference to Fig. 3. That is, even if the pore volume fractions in separate unit cells of similar form are the same, the ratio of the pore surface area to the unit cell volume is increased in proportion to the unit cell's edge length. Therefore, it can be expected that, if the volume of a unit cell become small, the effect of heat transfer via the pore surface is increased. In this sense, k_S is a material parameter associated with this effect and, in this study, is distinguished from k_∞ in (6). The introduction of this type of scale effect into the homogenization for the heat conduction problem in a porous medium is a new contribution of this work; otherwise the formulation is

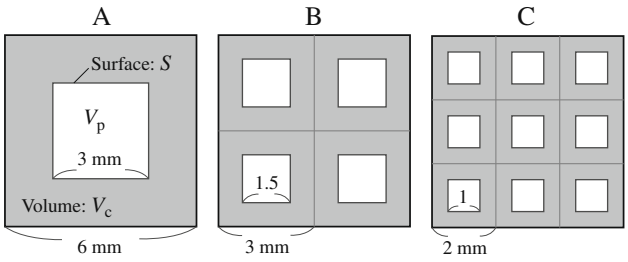

A	B	C
$\frac{V_p}{V_c}=\frac{9\times1}{36}=\frac{9}{36}$	$\frac{V_p}{V_c}=\frac{2.25\times4}{36}=\frac{9}{36}$	$\frac{V_p}{V_c}=\frac{1\times9}{36}=\frac{9}{36}$
$\frac{S}{V_c}=\frac{3\times4}{36}=\frac{12}{36}$	$\frac{S}{V_c}=\frac{1.5\times4\times4}{36}=\frac{24}{36}$	$\frac{S}{V_c}=\frac{1\times4\times9}{36}=\frac{36}{36}$

Fig. 3 Ratios of volume and surface of pores to the volume of representative volume elements of porous solids

ordinary, as in [5,6,21,11], and does not need to be presented here.

Using the formula (17), we obtain the following weak form:

$$\begin{aligned}
&\int_\Omega \frac{1}{|Y|}\int_{Y^\vartheta} c\rho\left(\bar{T}^0+\epsilon\bar{T}^1\right)\left(\dot{T}^0+\epsilon\dot{T}^1\right)dydx\\
&\quad+\int_\Omega \frac{1}{|Y|}\int_{Y^\vartheta}\left(\frac{1}{\epsilon}\nabla_y\bar{T}^0+\nabla_x\bar{T}^0+\nabla_y\bar{T}^1+\epsilon\nabla_x\bar{T}^1\right)\\
&\quad\cdot\boldsymbol{k}\left(\frac{1}{\epsilon}\nabla_y T^0+\nabla_x T^0+\nabla_y T^1+\epsilon\nabla_x T^1\right)dydx\\
&\quad+\int_{\Gamma_\infty} k_\infty\left(\bar{T}^0+\epsilon\bar{T}^1\right)\left(T^0+\epsilon T^1\right)d\Gamma\\
&\quad+\int_\Omega \frac{1}{|Y|}\int_S k_S\left(\bar{T}^0+\epsilon\bar{T}^1\right)\left(T^0+\epsilon T^1\right)d\Gamma dx\\
&=\int_\Omega \frac{1}{|Y|}\int_{Y^\vartheta}\left(\bar{T}^0+\epsilon\bar{T}^1\right)f dydx-\int_{\Gamma_q}\left(\bar{T}^0+\epsilon\bar{T}^1\right)\hat{p}d\Gamma\\
&\quad+\int_{\Gamma_\infty} k_\infty\left(\bar{T}^0+\epsilon\bar{T}^1\right)\hat{T}_\infty d\Gamma\\
&\quad+\int_\Omega \frac{1}{|Y|}\int_S k_S\left(\bar{T}^0+\epsilon\bar{T}^1\right)\hat{T}_S d\Gamma dx
\end{aligned}\tag{23}$$

where the last terms in both the left- and right-hand sides are of particular importance in the present study as mentioned above, since they represent the effect of heat transfer at the pore surfaces. Here, we have used the following formula for the integral over the pore surfaces in addition to the formula (17):

$$\lim_{\epsilon\to 0}\int_{S^\epsilon}\epsilon\varphi^\epsilon(\boldsymbol{x})d\Gamma=\int_\Omega\left[\frac{1}{|Y|}\int_S\varphi(\boldsymbol{x},\boldsymbol{y})dS\right]dx\tag{24}$$

The proof of this formula is found in [10,17]. It is this formula that the reason why weak formulations are employed in this study.

In this weak form (23), the identical equations with respect to the order of ϵ can be identified as follows:

- Order of ϵ^{-2}:

$$\int_\Omega \frac{1}{|Y|}\int_{Y^\vartheta}\nabla_y\bar{T}^0\cdot\boldsymbol{k}\nabla_y T^0 dydx=0\tag{25}$$

- Order of ϵ^{-1}:

$$\begin{aligned}
&\int_\Omega \frac{1}{|Y|}\int_{Y^\vartheta}\Big[\nabla_y\bar{T}^0\cdot\boldsymbol{k}\left(\nabla_x T^0+\nabla_y T^1\right)\\
&\quad+\left(\nabla_x\bar{T}^0+\nabla_y\bar{T}^1\right)\cdot\boldsymbol{k}\nabla_y T^0\Big]dydx=0
\end{aligned}\tag{26}$$

- Order of ϵ^0:

$$\begin{aligned}
&\int_\Omega \frac{1}{|Y|}\int_{Y^\vartheta} c\rho\bar{T}^0\dot{T}^0 dydx\\
&\quad+\int_\Omega \frac{1}{|Y|}\int_{Y^\vartheta}\Big[\nabla_y\bar{T}^0\cdot\boldsymbol{k}\nabla_x T^1+\nabla_x\bar{T}^1\cdot\boldsymbol{k}\nabla_y T^0\\
&\quad+\left(\nabla_x\bar{T}^0+\nabla_y\bar{T}^1\right)\cdot\boldsymbol{k}\left(\nabla_x T^0+\nabla_y T^1\right)\Big]dydx\\
&\quad+\int_{\Gamma_\infty} k_\infty\bar{T}^0T^0d\Gamma+\int_\Omega\frac{1}{|Y|}\int_S k_S\bar{T}^0T^0d\Gamma dx\\
&=\int_\Omega\frac{1}{|Y|}\int_{Y^\vartheta}\bar{T}^0 f dydx-\int_{\Gamma_q}\bar{T}^0\hat{p}d\Gamma\\
&\quad+\int_{\Gamma_\infty} k_\infty\bar{T}^0\hat{T}_\infty d\Gamma+\int_\Omega\frac{1}{|Y|}\int_S k_S\bar{T}^0\hat{T}_S d\Gamma dx
\end{aligned}\tag{27}$$

In the subsequent section, each equation is analyzed so that the two-scale heat conduction problem can be defined.

Equation (25) of order of ϵ^{-2} implies that

$$T^0=T^0(\boldsymbol{x})\quad(\text{ and }\ \bar{T}^0=\bar{T}^0(\boldsymbol{x})\ )\tag{28}$$

which guarantees (26) of order of ϵ^{-1} is automatically satisfied. Also, with (28) at hand, Eq. (27) of order of ϵ^0 becomes

$$\begin{aligned}
&\int_\Omega R^{\mathrm{H}}\bar{T}^0\dot{T}^0dx\\
&\quad+\int_\Omega\frac{1}{|Y|}\int_{Y^\vartheta}\left(\nabla_x\bar{T}^0+\nabla_y\bar{T}^1\right)\cdot\boldsymbol{k}\left(\nabla_x T^0+\nabla_y T^1\right)dydx\\
&\quad+\int_{\Gamma_\infty} k_\infty\bar{T}^0T^0d\Gamma+\int_\Omega k_S^{\mathrm{H}}\bar{T}^0T^0dx\\
&=\int_\Omega f^{\mathrm{H}}\bar{T}^0dx-\int_{\Gamma_q}\hat{p}\bar{T}^0d\Gamma\\
&\quad+\int_{\Gamma_\infty} k_\infty\bar{T}^0\hat{T}_\infty d\Gamma+\int_\Omega k_S^{\mathrm{H}}\bar{T}^0\hat{T}_S dx
\end{aligned}\tag{29}$$

Here, R^{H}, $f^{\mathrm{H}}(=\bar{f})$ and k_S^{H} are the average (or homogenized) heat capacity per unit volume, the average heat source/sink, and the homogenized heat transfer coefficient of the pore surfaces, respectively, and are defined as

$$R^{\mathrm{H}} = \frac{1}{|Y|}\int_{Y^\vartheta} c\rho \, dy = \langle c\rho \rangle \tag{30}$$

$$f^{\mathrm{H}} = \frac{1}{|Y|}\int_{Y^\vartheta} f \, dy = \langle f \rangle \tag{31}$$

$$k_S^{\mathrm{H}} = \frac{1}{|Y|}\int_{S} k_S \, d\Gamma \tag{32}$$

where we have introduced a bracket operator as

$$\langle \bullet \rangle := \frac{1}{|Y|}\int_{Y^\vartheta} \bullet \, dy \tag{33}$$

to indicate the volume average for the RVE. It should be noted that the last terms in both the left- and right-hand sides in (29) are volume integrals, even though the expression (32) for k_S^{H} is a surface integral in the micro-scale.

If the variation is taken as $\bar{T}^1 = \bar{T}^0(\boldsymbol{x})$ in (29), the following macroscopic governing equation for the solution $T^0(\boldsymbol{x}, t) \in \mathcal{U}_T$ can be identified:

$$\begin{aligned}
&\int_\Omega R^{\mathrm{H}} \bar{T}^0 \dot{T}^0 dx \\
&\quad + \int_\Omega \nabla_x \bar{T}^0 \cdot \frac{1}{|Y|}\int_{Y^\vartheta} \boldsymbol{k}\left(\nabla_x T^0 + \nabla_y T^1\right) dy dx \\
&\quad + \int_{\Gamma_\infty} k_\infty \bar{T}^0 T^0 d\Gamma + \int_\Omega k_S^{\mathrm{H}} \bar{T}^0 T^0 dx \\
&= \int_\Omega f^{\mathrm{H}} \bar{T}^0 dx - \int_{\Gamma_q} \hat{p} \bar{T}^0 d\Gamma \\
&\quad + \int_{\Gamma_\infty} k_\infty \bar{T}^0 \hat{T}_\infty d\Gamma + \int_\Omega k_S^{\mathrm{H}} \bar{T}^0 \hat{T}_S dx \quad \forall \bar{T}^0 \in \mathcal{V}_T
\end{aligned} \tag{34}$$

where, for the sake of simplicity, the function set and space, $\mathcal{U}_T$ and $\mathcal{V}_T$, are the same as those used in the original problem in (8). Putting this back to (29), we can obtain the following microscopic governing equation:

$$\begin{aligned}
&\int_\Omega \frac{1}{|Y|}\int_{Y^\vartheta} \nabla_y \bar{T}^1 \cdot \boldsymbol{k}\left(\nabla_x T^0 + \nabla_y T^1\right) dy dx = 0 \\
&\forall \bar{T}^1 \in \tilde{\mathcal{V}}_T^{\mathrm{per}}.
\end{aligned} \tag{35}$$

Here, $\tilde{\mathcal{V}}_T^{\mathrm{per}}$ is the subspace of $\mathcal{V}_T^{\mathrm{per}}$ such that

$$\tilde{\mathcal{V}}_T^{\mathrm{per}} = \left\{ T^*(\bullet; \boldsymbol{y}) \in \mathcal{V}_T^{\mathrm{per}} \middle| \int_Y T^*(\bullet; \boldsymbol{y}) dy = 0 \right\} \tag{36}$$

where $\mathcal{V}_T^{\mathrm{per}}$ is a relevant function space of Y-periodic functions.

Equations (34) and (35) just derived are the governing equations for the two-scale heat conduction problem. It is to be noted that the coupling between micro- and macro-scale behaviors arises from the temperature gradient term

$$\nabla_y z(\boldsymbol{x}, \boldsymbol{y}, t) = \nabla_x T^0(\boldsymbol{x}, t) + \nabla_y T^1(\boldsymbol{x}, \boldsymbol{y}, t) \tag{37}$$

where $z(\boldsymbol{x}, \boldsymbol{y})$ is the actual temperature field in the RVE. The macroscopic equation (34) is solved for the macroscopic temperature field $T^0(\boldsymbol{x})$ in Ω with the microscopic Y-periodic temperature field $T^1(\boldsymbol{x}, \boldsymbol{y})$ given as a datum, while the microscopic equation (35) is for $T^1(\boldsymbol{x}, \boldsymbol{y})$ in Y^ϑ at each macroscopic point $\boldsymbol{x}$ with $T^0(\boldsymbol{x})$ given as a datum.

3.2.2 Homogenizaion for the heat conduction problem

The micro-scale Y-periodic temperature field $T^1(\boldsymbol{x}, \boldsymbol{y}, t)$ can be assumed to be in proportion to the macro-scale temperature gradient so that

$$T^1(\boldsymbol{x}, \boldsymbol{y}, t) = -\zeta^j(\boldsymbol{y}) \frac{\partial T^0(\boldsymbol{x}, t)}{\partial x_j} + \tilde{T}^1(\boldsymbol{x}) \tag{38}$$

where ζ^j $(j = 1, 2, 3)$ are called the characteristic functions and are Y-periodic scalar-valued functions with units of length in response to three patterns of unit macro-scale temperature gradient, which will be defined later. Here, $\tilde{T}^1(\boldsymbol{x})$ is an indefinite constant, but can be set at zero due to the restriction in (36) for T^1 (and ζ^j) such that

$$\int_Y T^1(\boldsymbol{x}, \boldsymbol{y}) \, dy = 0 \quad \Rightarrow \quad \tilde{T}^1(\boldsymbol{x}) = 0 \tag{39}$$

Substitution of (38) for T^1 into (35) yields the following weak form at each macro-scale material point $\boldsymbol{x}$:

$$\begin{aligned}
&\int_{Y^\vartheta} \nabla_y \bar{T}^1 \cdot \boldsymbol{k} \nabla_y \zeta^j \, dy = \int_{Y^\vartheta} \nabla_y \bar{T}^1 \cdot \boldsymbol{k} \mathbf{1}^j \, dy \\
&\forall \bar{T}^1 \in \tilde{\mathcal{V}}_T^{\mathrm{per}}, \quad j = 1, 2, 3
\end{aligned} \tag{40}$$

where $\mathbf{1}^j$ are three unit vectors of the macroscopic temperature gradient with its jth component being 1 and with others being 0. On the other hand, by substituting (38) into the macroscopic governing equation (34), we can eliminate the term involving T^1 from the macroscopic governing equation for T^0 such that

$$\begin{aligned}
&\int_\Omega R^{\mathrm{H}} \bar{T}^0 \dot{T}^0 \, dx + \int_\Omega \nabla_x \bar{T}^0 \cdot \boldsymbol{k}^{\mathrm{H}} \nabla_x T^0 \, dx \\
&\quad + \int_{\Gamma_\infty} k_\infty \bar{T}^0 T^0 \, d\Gamma + \int_\Omega k_S^{\mathrm{H}} \bar{T}^0 T^0 \, dx
\end{aligned}$$

$$= \int_\Omega f^{\mathrm{H}} \bar{T}^0 \, dx - \int_{\Gamma_q} \hat{p} \bar{T}^0 \, d\Gamma + \int_{\Gamma_\infty} k_\infty \bar{T}^0 \hat{T}_\infty \, d\Gamma + \int_\Omega k_S^{\mathrm{H}} \bar{T}^0 \hat{T}_S \, dx \quad \forall \bar{T}^0 \in \mathcal{V}_T \tag{41}$$

In this expression, we have defined the homogenized heat conduction tensor $\boldsymbol{k}^{\mathrm{H}}$ as

$$\boldsymbol{k}^{\mathrm{H}} = \frac{1}{|Y|} \int_{Y^\vartheta} \boldsymbol{k} \cdot \left(\boldsymbol{I} - \nabla_y \boldsymbol{\zeta} \right) dy \tag{42}$$

where $\boldsymbol{I}$ is the second-order identity tensor and $\boldsymbol{\zeta} = \left\{ \zeta^1 \ \zeta^2 \ \zeta^3 \right\}^{\mathrm{T}}$.

In summary, the strong form corresponding to the weak form (41) can be written as follows:

$$R^{\mathrm{H}} \dot{T}^0 = -\nabla_x \cdot \boldsymbol{Q} + f^{\mathrm{H}} - k_S^{\mathrm{H}} (T^0 - \hat{T}_S) \quad \text{in } \Omega \tag{43}$$

$$\boldsymbol{Q} = -\boldsymbol{k}^{\mathrm{H}} \boldsymbol{V} \quad \text{in } \Omega \tag{44}$$

$$\boldsymbol{V} = \nabla T^0 \quad \text{in } \Omega \tag{45}$$

along with the boundary conditions

$$T^0 = \hat{T} \quad \text{on } \Gamma_T \tag{46}$$

$$\boldsymbol{Q} \cdot \boldsymbol{n} = \hat{p} \quad \text{on } \Gamma_q \tag{47}$$

$$\boldsymbol{Q} \cdot \boldsymbol{n} = k_\infty (T^0 - \hat{T}_\infty) \quad \text{on } \Gamma_\infty \tag{48}$$

and the initial condition

$$T^0(\boldsymbol{x}, 0) = T_0(\boldsymbol{x}) \quad \text{in } \Omega \tag{49}$$

It is to be noted here that the heat transfer via pore sufaces is realized as the heat supply in the source/sink term of (43) at each macroscopic point, according its temperature value.

3.2.3 Localization for heat conduction problem

The solution procedure to obtain the microscopic response with the macroscopic solution as a datum is commonly referred to as 'localization' within the framework of the mathematical homogenization [6]. For the two-scale heat conduction problem, if necessary, the localization can be performed with the macroscopic temperature gradient to obtain the micro-scale temperature field as well as heat flux.

For this purpose, we first define the macroscopic temperature gradient as $\boldsymbol{V}(\boldsymbol{x}, t) = \nabla_x T^0$ and re-write the microscopic temperature gradient (37) as

$$\nabla_y z(\boldsymbol{x}, \boldsymbol{y}, t) = \boldsymbol{V}(\boldsymbol{x}, t) + \nabla_y T^1(\boldsymbol{x}, \boldsymbol{y}, t) \tag{50}$$

When this is integrated in space, the microscopic temperature field becomes

$$z(\boldsymbol{x}, \boldsymbol{y}, t) = \boldsymbol{V}(\boldsymbol{x}, t) \cdot \boldsymbol{y} + T^1(\boldsymbol{x}, \boldsymbol{y}, t) + \tilde{T}^z(\boldsymbol{x}, t) \tag{51}$$

where $\tilde{T}^z(\boldsymbol{x}, t)$ is an integration constant and represents an indefinite function of $\boldsymbol{x}$. In order to determine $\tilde{T}^z(\boldsymbol{x}, t)$, we postulate that the volume average of the micro-scale temperature field $z(\boldsymbol{x}, \boldsymbol{y}, t)$ be the macroscopic temperature field $T^0(\boldsymbol{x}, t)$ as

$$\langle z(\boldsymbol{x}, \boldsymbol{y}, t) \rangle = \frac{1}{|Y|} \int_{Y^\vartheta} z(\boldsymbol{x}, \boldsymbol{y}, t) \, dy = T^0(\boldsymbol{x}, t) \tag{52}$$

Since $T^1(\boldsymbol{x}, \boldsymbol{y}, t)$ is in $\tilde{\mathcal{V}}_T^{\mathrm{per}}$ with the relation (39), the indefinite term $\tilde{T}^z(\boldsymbol{x})$ can be of the following form:

$$\tilde{T}^z(\boldsymbol{x}, t) = T^0(\boldsymbol{x}, t) - \boldsymbol{V}(\boldsymbol{x}, t) \cdot \langle \boldsymbol{y} \rangle \tag{53}$$

Together with the micro-scale Y-periodic temperature field $T^1(\boldsymbol{x}, \boldsymbol{y}, t)$ in the form of (38), the actual microscopic temperature field $z(\boldsymbol{x}, \boldsymbol{y}, t)$ in the unit cell becomes

$$z(\boldsymbol{x}, \boldsymbol{y}, t) = \boldsymbol{V}(\boldsymbol{x}, t) \cdot (\boldsymbol{y} - \boldsymbol{\zeta}(\boldsymbol{y}) - \langle \boldsymbol{y} \rangle) + T^0(\boldsymbol{x}, t) \tag{54}$$

where $\boldsymbol{\zeta} = \left\{ \zeta^1 \ \zeta^2 \ \zeta^3 \right\}^{\mathrm{T}}$ as defined above. When the origin of the micro-scale coordinate system is placed at the center of the unit cell so that $\langle \boldsymbol{y} \rangle = \boldsymbol{0}$, the forth term can be eliminated, if necessary.

In spite of this formulation, the first three terms in (54) neither make sense nor have effects on the deformation of the solid phase under the assumption made before that the micro-scale temperature distribution becomes steady-state instantaneously.

3.3 Two-scale deformation problem with thermal expansion/contraction

By applying the method of asymptotic expansions, we derive the micro- and macroscopic governing equations that define the two-scale deformation problem with thermal expansion/contraction. The procedure is almost the same as that described above for the heat conduction problem, and is ndependent of it. However, since the formulation is not fresh and has already been reported elsewhere in the literature [9,17], we here start with the intermediate equations derived by assuming the asymptotically expanded forms of the displacement field and its variation as

$$\boldsymbol{u}^\epsilon(\boldsymbol{x}, t) = \boldsymbol{u}^0(\boldsymbol{x}, \boldsymbol{y}, t) + \epsilon \boldsymbol{u}^1(\boldsymbol{x}, \boldsymbol{y}, t) + \epsilon^2 \boldsymbol{u}^2(\boldsymbol{x}, \boldsymbol{y}, t) + \cdots \tag{55}$$

$$\bar{\boldsymbol{u}}^\epsilon(\boldsymbol{x}) = \bar{\boldsymbol{u}}^0(\boldsymbol{x}, \boldsymbol{y}) + \epsilon \bar{\boldsymbol{u}}^1(\boldsymbol{x}, \boldsymbol{y}) + \epsilon^2 \bar{\boldsymbol{u}}^2(\boldsymbol{x}, \boldsymbol{y}) + \cdots \tag{56}$$

along with, in view of (18) and (19),

$$\theta^\epsilon(\boldsymbol{x}, t) = \theta^0(\boldsymbol{x}, t) + \epsilon \theta^1(\boldsymbol{x}, \boldsymbol{y}, t) + \epsilon^2 \theta^2(\boldsymbol{x}, \boldsymbol{y}, t) + \cdots \tag{57}$$

Here, needless to say, t in (55) is real time, even though quasi-static deformation processes are assumed, and the time marching is brought by the temperature change in (57).

The micro- and macroscopic governing equations are respectively derived as follows:

– Macro-scale: Given $\boldsymbol{u}^1$, find $\boldsymbol{u}^0 \in \mathcal{U}_u$ such that

$$\int_\Omega \nabla_x^{(\mathrm{s})}\bar{\boldsymbol{u}}^0 : \frac{1}{|Y|}\int_{Y^\vartheta} \boldsymbol{c} : \left(\nabla_x^{(\mathrm{s})}\boldsymbol{u}^0 + \nabla_y^{(\mathrm{s})}\boldsymbol{u}^1\right) dydx = \int_\Omega \nabla_x^{(\mathrm{s})}\bar{\boldsymbol{u}}^0 : \frac{1}{|Y|}\int_{Y^\vartheta} \theta^0\boldsymbol{\beta}\, dydx + \int_\Omega \bar{\boldsymbol{u}}^0\cdot\rho^{\mathrm{H}}\hat{\boldsymbol{b}}\, dx + \int_{\Gamma_t}\bar{\boldsymbol{u}}^0\cdot\hat{\boldsymbol{t}}\, d\Gamma \quad \forall\bar{\boldsymbol{u}}^0\in\mathcal{V}_u \tag{58}$$

– Micro-scale: Given $\boldsymbol{u}^0$, find $\boldsymbol{u}^1 \in \tilde{\mathcal{V}}_u^{\mathrm{per}}$ such that

$$\int_\Omega \frac{1}{|Y|}\int_{Y^\vartheta} \nabla_y^{(\mathrm{s})}\bar{\boldsymbol{u}}^1 : \boldsymbol{c} : \left(\nabla_x^{(\mathrm{s})}\boldsymbol{u}^0 + \nabla_y^{(\mathrm{s})}\boldsymbol{u}^1\right) dydx = \int_\Omega \frac{1}{|Y|}\int_{Y^\vartheta} \nabla_y^{(\mathrm{s})}\bar{\boldsymbol{u}}^1 : \theta^0\boldsymbol{\beta}\, dydx \quad \forall\bar{\boldsymbol{u}}^1\in\tilde{\mathcal{V}}_u^{\mathrm{per}} \tag{59}$$

where $\boldsymbol{u}^0$ is the macroscopic displacement field, $\boldsymbol{u}^1$ is the microscopic Y-periodic displacement field, ρ^{H} is the average mass density defined as

$$\rho^{\mathrm{H}} = \frac{1}{|Y|}\int_{Y^\vartheta}\rho\, dy = \langle\rho\rangle \tag{60}$$

It is to be noted that the temperature change in (58) and (59) is defined as $\theta^0(\boldsymbol{x},t) = T^0(\boldsymbol{x},t) - T_0(\boldsymbol{x})$ and is constant in a unit cell. That is, the temperature change causing thermal expansion/contraction is a macroscopic quantity. This means that the micro-scale temperature change in time due to the change of the macroscopic temperature gradient $\boldsymbol{V}$ in (54) is negligibly small compared with the change of the absolute value of $T_0(\boldsymbol{x})$; that is, within a time interval $[t, t+\Delta t]$,

$$\begin{aligned} &z(\boldsymbol{x},\boldsymbol{y},t+\Delta t) - z(\boldsymbol{x},\boldsymbol{y},t) \\ &= (\boldsymbol{V}(\boldsymbol{x},t+\Delta t) - \boldsymbol{V}(\boldsymbol{x},t))\,(\boldsymbol{y}-\boldsymbol{\zeta}(\boldsymbol{y}) - \langle\boldsymbol{y}\rangle) \\ &\quad + T^0(\boldsymbol{x},t+\Delta t) - T^0(\boldsymbol{x},t) \qquad (61)\\ &\approx T^0(\boldsymbol{x},t+\Delta t) - T^0(\boldsymbol{x},t) := \theta^0(\boldsymbol{x},t) \qquad (62)\end{aligned}$$

This is true when the unit cell is infinitesimally small, which is consistent with our assumption in this study.

3.3.1 Homogenization for deformation problem with thermal expansion/contraction

The micro-scale Y-periodic displacement field $\boldsymbol{u}^1(\boldsymbol{x},\boldsymbol{y},t)$ in (58) and (59) can be assumed to be of the form

$$\boldsymbol{u}^1(\boldsymbol{x},\boldsymbol{y},t) = -\boldsymbol{\chi}^{kh}(\boldsymbol{y})E_{kh}(\boldsymbol{x},t) + \theta^0\boldsymbol{\psi}(\boldsymbol{y}) \tag{63}$$

where θ^0 is the macro-scale temperature change, and $\boldsymbol{E} = E_{ij}\boldsymbol{e}_i\otimes\boldsymbol{e}_j = \nabla_x^{(\mathrm{s})}\boldsymbol{u}^0$ is the macroscopic strain with $\boldsymbol{e}_i$ $(i=1,2,3)$ being the basis vectors in macro-scale. Here, $(k,h) = \{(1,1),(2,2),(3,3),(1,2),(2,3),(3,1)\}$ in $\boldsymbol{\chi}^{kh}$ are the Y-periodic characteristic displacement vectors in response to six mutually-independent fundamental patterns of unit macroscopic strains, which only the kh-component is unity. Also, $\boldsymbol{\psi}$ is the Y-periodic characteristic displacement vector in response to unit temperature change for thermal expansion/contraction. By substituting (63) into (59), we obtain the following equations for the characteristic displacement vectors, $\boldsymbol{\chi}^{kh}$ and $\boldsymbol{\psi}$, respectively:

$$\int_{Y^\vartheta}\nabla_y^{(\mathrm{s})}\bar{\boldsymbol{u}}^1 : \boldsymbol{c} : \nabla_y^{(\mathrm{s})}\boldsymbol{\chi}^{kh}\, dy = \int_{Y^\vartheta}\nabla_y^{(\mathrm{s})}\bar{\boldsymbol{u}}^1 : \boldsymbol{c} : \boldsymbol{I}^{kh}\, dy \quad \forall\bar{\boldsymbol{u}}^1\in\tilde{\mathcal{V}}_u^{\mathrm{per}} \tag{64}$$

$$\int_{Y^\vartheta}\nabla_y^{(\mathrm{s})}\bar{\boldsymbol{u}}^1 : \boldsymbol{c} : \nabla_y^{(\mathrm{s})}\boldsymbol{\psi}\, dy = \int_{Y^\vartheta}\nabla_y^{(\mathrm{s})}\bar{\boldsymbol{u}}^1 : \boldsymbol{\beta}\, dy \quad \forall\bar{\boldsymbol{u}}^1\in\tilde{\mathcal{V}}_u^{\mathrm{per}} \tag{65}$$

where $\boldsymbol{I}^{kh}$ is the second-order tensors of unit macroscopic strain, whose components are identified in

$$\boldsymbol{I}^{kh} = \frac{1}{2}\left(\delta_{ki}\delta_{hj} + \delta_{hi}\delta_{kj}\right)\boldsymbol{e}_i\otimes\boldsymbol{e}_j \tag{66}$$

We substitute the expression (63) for $\boldsymbol{u}^1$ into the macroscopic weak form (58) to arrive at the following equation for the macroscopic displacement field $\boldsymbol{u}^0\in\mathcal{U}_u$:

$$\int_\Omega \nabla_x^{(\mathrm{s})}\bar{\boldsymbol{u}}^0 : \boldsymbol{c}^{\mathrm{H}} : \nabla_x^{(\mathrm{s})}\boldsymbol{u}^0\, dx = \int_\Omega \nabla_x^{(\mathrm{s})}\boldsymbol{u}^0 : \theta^0\boldsymbol{\beta}^{\mathrm{H}}\, dx + \int_\Omega \bar{\boldsymbol{u}}^0\cdot\rho^{\mathrm{H}}\hat{\boldsymbol{b}}\, dx + \int_{\Gamma_t}\bar{\boldsymbol{u}}^0\cdot\hat{\boldsymbol{t}}\, d\Gamma \quad \forall\bar{\boldsymbol{u}}^0\in\mathcal{V}_u \tag{67}$$

where $\boldsymbol{c}^{\mathrm{H}}$ and $\boldsymbol{\beta}^{\mathrm{H}}$ are the homogenized elasticity tensor of the forth order and the homogenized thermal expansion stress per unit temperature change, respectively, and are defined as

$$\boldsymbol{c}^{\mathrm{H}} = \frac{1}{|Y|}\int_{Y^\vartheta} c_{ijlm}\left(I_{lm}^{kh} - \frac{\partial\chi_l^{kh}}{\partial y_m}\right)dy\,\left(\boldsymbol{e}_i\otimes\boldsymbol{e}_j\otimes\boldsymbol{e}_k\otimes\boldsymbol{e}_h\right) \tag{68}$$

$$\boldsymbol{\beta}^{\mathrm{H}} = \frac{1}{|Y|}\int_{Y^\vartheta}\left(\boldsymbol{\beta} - \boldsymbol{c} : \nabla_y^{(\mathrm{s})}\boldsymbol{\psi}\right)dy \tag{69}$$

In summary, the strong form corresponding to the weak form (67) can be written as follows:

$$\nabla_x\cdot\boldsymbol{\Sigma} + \rho^{\mathrm{H}}\hat{\boldsymbol{b}} = \boldsymbol{0} \quad \text{in } \Omega \tag{70}$$

$$\boldsymbol{E} = \frac{1}{2}\left\{\nabla_x\boldsymbol{u}^0 + \boldsymbol{u}^0\nabla_x\right\} = \nabla_x^{(\mathrm{s})}\boldsymbol{u}^0 \quad \text{in } \Omega \tag{71}$$

$$\boldsymbol{\Sigma} = \boldsymbol{c}^{\mathrm{H}} : \boldsymbol{E} - \theta^0\boldsymbol{\beta}^{\mathrm{H}} = \boldsymbol{c}^{\mathrm{H}} : \left(\boldsymbol{E} - \theta^0\boldsymbol{\alpha}^{\mathrm{H}}\right) \quad \text{in } \Omega \tag{72}$$

along with the boundary conditions

$$\boldsymbol{u}^0 = \hat{\boldsymbol{u}} \quad \text{on } \Gamma_u \tag{73}$$

$$\boldsymbol{\Sigma n} = \hat{\boldsymbol{t}} \quad \text{on } \Gamma_t \tag{74}$$

Here, we have defined the macroscopic stress as $\boldsymbol{\Sigma} := \langle \boldsymbol{\sigma} \rangle$ and the homogenized coefficient of thermal expansions as

$$\boldsymbol{\alpha}^{\mathrm{H}} := (\boldsymbol{c}^{\mathrm{H}})^{-1} \boldsymbol{\beta}^{\mathrm{H}}. \tag{75}$$

3.3.2 Localization for deformation problem with thermal expansion/contraction

Denoting the actual micro-scale displacement in the unit cell by $\boldsymbol{w}(\boldsymbol{x}, \boldsymbol{y}, t)$, we write the micro-scale strain as

$$\nabla_y^{(\mathrm{s})} \boldsymbol{w}(\boldsymbol{x}, \boldsymbol{y}, t) = \nabla_x^{(\mathrm{s})} \boldsymbol{u}^0(\boldsymbol{x}, t) + \nabla_y^{(\mathrm{s})} \boldsymbol{u}^1(\boldsymbol{x}, \boldsymbol{y}, t) \tag{76}$$

Then the $\boldsymbol{w}(\boldsymbol{x}, \boldsymbol{y}, t)$ is obtained as

$$\boldsymbol{w}(\boldsymbol{x}, \boldsymbol{y}, t) = \boldsymbol{E}(\boldsymbol{x}, t) \cdot \boldsymbol{y} + \boldsymbol{u}^1(\boldsymbol{x}, \boldsymbol{y}, t) + \tilde{\boldsymbol{u}}^w(\boldsymbol{x}, t) \tag{77}$$

where an indefinite term $\tilde{\boldsymbol{u}}^w(\boldsymbol{x}, t)$ is constant with respect to the micro-scale and can be neglected without loss of generality, because it has no effect on the values of the microscopic strain and stress components. The substitution of the expression (63) for $\boldsymbol{u}^1(\boldsymbol{x}, \boldsymbol{y}, t)$ into (77) yields

$$\begin{aligned} &\boldsymbol{w}(\boldsymbol{x}, \boldsymbol{y}, t) \\ &= \boldsymbol{E}(\boldsymbol{x}, t) \cdot \boldsymbol{y} - \boldsymbol{\chi}^{kh}(\boldsymbol{y}) E_{kh}(\boldsymbol{x}, t) + \theta^0(\boldsymbol{x}, t) \boldsymbol{\psi}(\boldsymbol{y}) \\ &= \left[\left(\delta_{ik} \delta_{jh} y_j - \chi_i^{kh}(\boldsymbol{y}) \right) E_{kh}(\boldsymbol{x}, t) + \theta^0(\boldsymbol{x}, t) \psi_i(\boldsymbol{y}) \right] \boldsymbol{e}_i \end{aligned} \tag{78}$$

4 Numerical verification of two-scale thermo-mechanical model for porous solid

We conduct a numerical verification of the proposed two-scale thermo-mechanical coupled model for porous solids derived above. The model problem considered here is simple, but illustrative enough to demonstrate the relevancy of the present formulation.

4.1 Analysis models, conditions and cases

The analysis model is a rectangular parallelepiped structure shown in Fig. 4, which is composed of periodically arranged, cubic microstructures (unit cells) with mutually connected pores. In order to elucidate the effect of heat transfer at pore surfaces, we consider the fluid phase in pores as a medium that transports heat. The material parameters for the solid and fluid phases are provided in Table 1.

The concrete assumptions and analytical conditions made for the thermo-mechanical coupling analysis are itemized as follows:

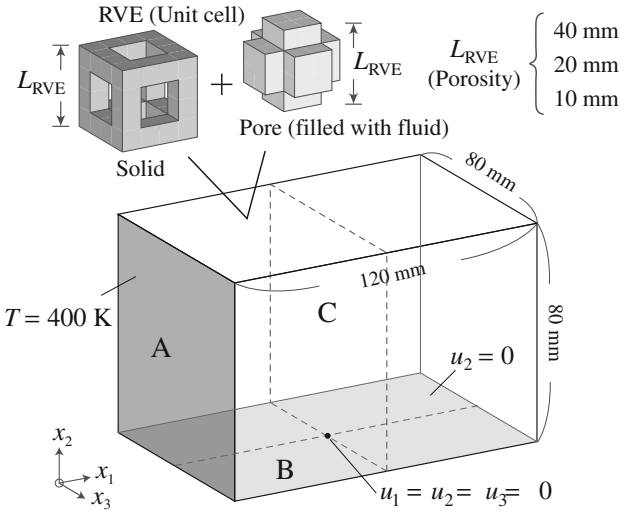

Fig. 4 Macro-structure and unit cell of a porous medium along with boundary conditions for displacement and temperature: pores are filled with fluid

Table 1 Material parameters for solid and fluid phases

	Solid	Fluid
Young's modulus (MPa)	10,000	–
Poisson's ratio	0.20	–
Density (kg/m^3)	2,000	1,000
Thermal expansion coef. (1/K)	0.00001	–
Heat conduction coef. (W/mmK)	0.01	0.04
Specific heat (J/kgK)	100	400
Heat transfer coef. (W/mm^{2}K)	0.00001	0.0

[Assumptions]

- Adiabatic condition is imposed on the external boundaries of the solid phase.
- Fluid flow is not allowed in the fluid phase.
- The fluid phase does not sustain stress, and is neither expanded nor contracted with temperature change.
- Heat is transferred to the solid phase from the fluid phase only at the pore surfaces, namely at their interfaces.
- Heat is not transferred to the fluid phase from the solid phase, implying that the heat transfer coefficient of the fluid is zero.

[Analytical conditions]

- There is no mechanical loading on the solid phase; that is, only the thermal loading is considered.
- Displacement is prescribed on the bottom surface (Surface B) as indicated in Fig. 4.
- Heat is given to the external boundaries of the fluid phase only and is conducted in it with its own heat conductiv-

ity; temperature 400 K is prescribed on Surface A of the macro-structure; see Fig. 4.
– Initial temperature 300 K is given to both the solid and the fluid phases.

Although the fluid flow is not considered in this numerical example, it can be expected from the present setting that the proposed two-scale thermo-mechanical coupled model can be applied to a stress analysis of porous solids subjected to heat transport by fluid advection.

In order to see the scale effect due to heat transfer via pore surfaces, we consider three sizes of unit cells that have the same volume fraction of pore; $L_{\mathrm{RVE}} = 40,\ 20,\ 10$ mm; see Fig. 4. Thus, three separate macro-scale coupling analyses are carried out after the micro-scale analysis to evaluate homogenized material properties. The average properties $\boldsymbol{c}^{\mathrm{H}}$, $\boldsymbol{\alpha}^{\mathrm{H}}$, ρ^{H}, $\boldsymbol{k}^{\mathrm{H}}$, R^{H}, f^{H} defined in Sect. 3 are the same for these three unit cell models, but the higher the ratio of the pore surface area to the unit cell volume, the larger the homogenized heat transfer coefficient k_S^{H} defined in (32), as estimated in Sect. 3.2. The numerical analyses with these homogenized properties based on the proposed formulation are referred to as "two-scale analyses" in this study.

The finite element (FE) meshes for the two-scale thermo-mechanical analyses are all generated with standard 8-node hexahedral elements and are presented in Fig. 5. The three unit cell models of different edge lengths as $L_{\mathrm{RVE}} = 40$, 20, 10 mm are separately prepared, while the common macro model is used for the solid and fluid phases. In what follows, the analysis models or cases corresponding to these unit cell models are denoted by HOM-40, HOM-20 and HOM-10. The heat transfer coefficient k_S of the integrand of (32) is set at 0.00001 W/mm^2 K as in Table 1 and is common to all the unit cell models.

It should be noted that the pores are assumed to be infinitesimally small in formulating the proposed mathematical model by the application of the asymptotic homogenization method, though actual porous media inevitably have finitely sized unit cells. To validate such a model, we also obtain the reference solutions for comparison by carrying out single-scale analyses of porous media without homogenization; in other words, we solve the original problems in Sect. 2. The numerical analyses for this set of reference solutions are referred to as "direct analyses" in this study.

The FE meshes prepared for the direct analyses are generated with standard tri-linear hexahedral elements and are shown in Fig. 6 ($L_{\mathrm{RVE}} = 40$ mm), Fig. 7 ($L_{\mathrm{RVE}} = 20$ mm) and Fig. 8 ($L_{\mathrm{RVE}} = 10$ mm), for which the boundary conditions indicated in Fig. 4 and the material parameters in Table 1 are directly applied. Note here that the number of elements and other conditions for a single unit cell in these models are in accordance with those of the corresponding unit cell prepared above for the two-scale analyses. The heat transfer

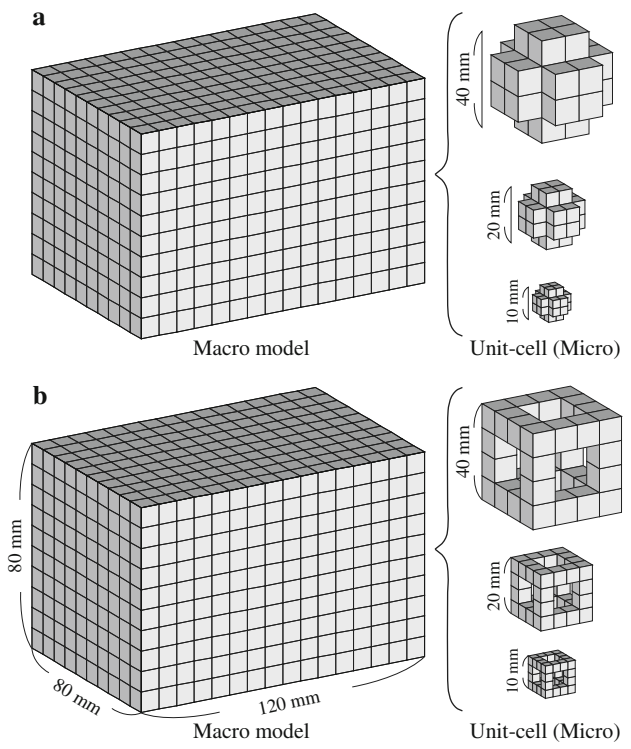

Fig. 5 Corresponding homogenized model with differently-sized unit-cell (HOM-40, HOM-20, HOM-10): **a** homogenized finite element model of fluid phase; **b** homogenized finite element model of solid phase

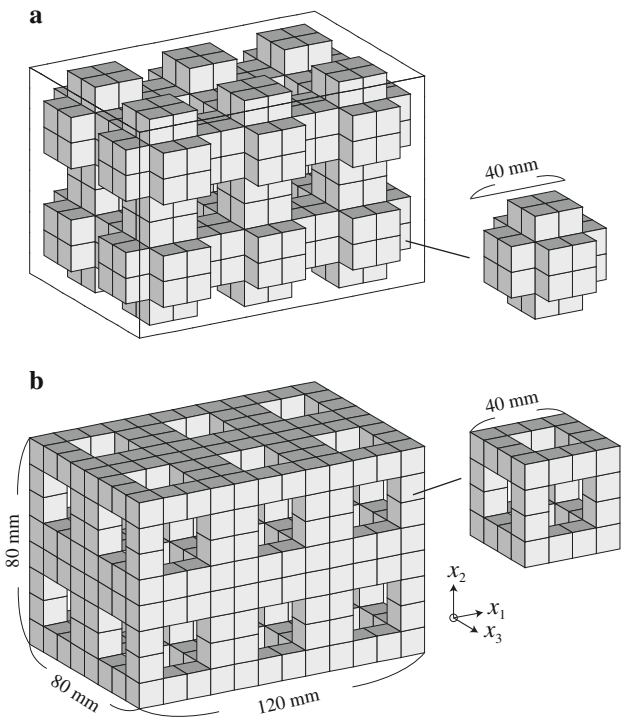

Fig. 6 Direct model with $L_{\mathrm{RVE}} = 40$ (DIR-40): **a** direct finite element model of fluid phase; **b** direct finite element model of solid phase

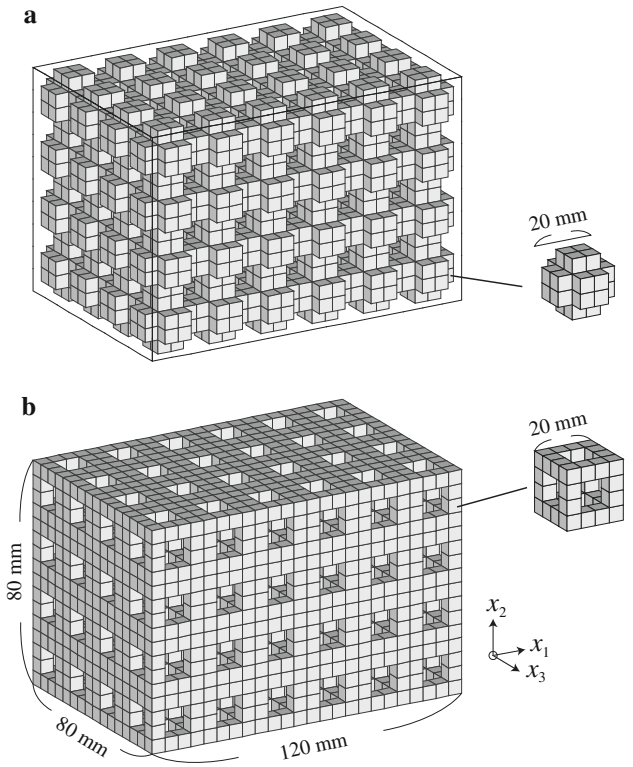

Fig. 7 Direct model with $L_{\mathrm{RVE}} = 20$ (DIR-20): **a** direct finite element model of fluid phase; **b** direct finite element model of solid phase

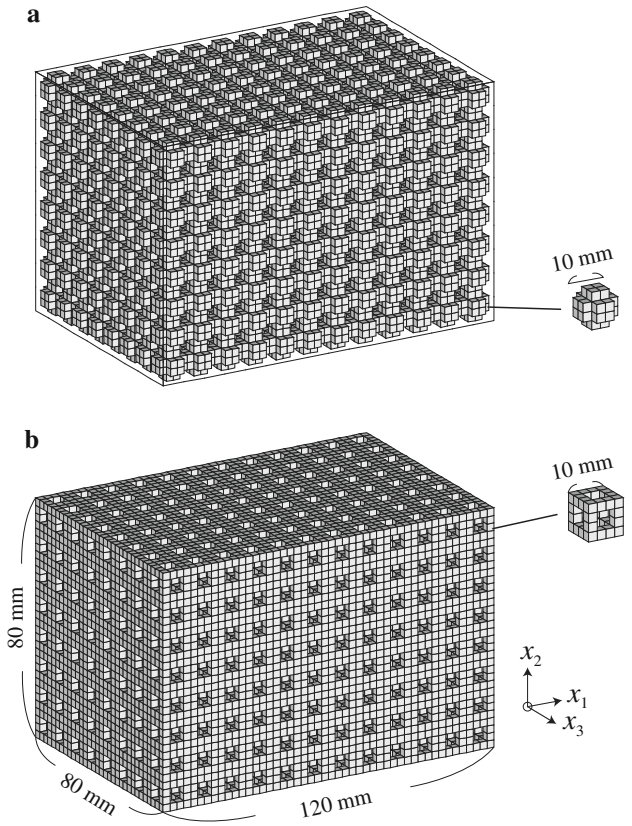

Fig. 8 Direct model with $L_{\mathrm{RVE}} = 10$ (DIR-10): **a** direct finite element model of fluid phase; **b** direct finite element model of solid phase

coefficient of the pore surfaces k_S^{ϵ} in (7) is assumed to be the same as k_∞ in (6) and is set at 0.00001 W/mm^2 K. In what follows, the three numerical models prepared for direct analyses are respectively denoted by DIR-40, DIR-20 and DIR-10 with reference to the corresponding edge lengths of unit cells, L_{RVE}.

4.2 Solution method and numerical algorithm

We employ a weak coupling solution method for both two-scale and direct analyses of the unsteady thermo-mechanical coupling problem and, as originally assumed, the coupling is one way from the transient heat conduction problem to the quasi-static deformation problem. That is, each problem is solved separately, and the solution of the heat conduction problem is given to the deformation problem unilaterally.

The standard Crank–Nicolson method is employed to solve the unsteady heat conduction problem along with the setting provided above, and a time period of 200 s is discredited into 100 time steps. The deformation problem is solved at each time step, which is set for the heat conduction problem, with the solution of the heat conduction problem being the data for evaluating thermal expansion/contraction of the solid phase.

We adopt the following computational procedure for the direct analyses:

(1) Start the time stepping procedure.
(2) Solve the heat conduction problem of the fluid phase with the initial and boundary conditions given above to obtain the temperature distribution that is used for the boundary data at the pore surfaces of the solid phase.
(3) Solve the heat conduction problem of the solid phase by applying the boundary conditions. Here, only the temperature values on the pore surfaces are assumed to change with time.
(4) Using the temperature distribution in the solid phase evaluated in Step (3), calculate the strain and stress in the solid phase due to thermal expansion/contraction.
(5) Solve the deformation problem along with the boundary conditions given and the "initial stress", as evaluated in Step (4).
(6) Set the time step forward and go back to Step (2).

The two-scale analyses are conducted in accordance with the following computational procedure:

(1) Before starting the time stepping procedure, evaluate all the effective material properties of the solid and fluid phases used for the two-scale thermo-mechanical problem. For both the fluid and solid phases,

– the average mass density, heat capacity and heat source are calculated, and
– the homogenized heat conduction tensor is evaluated by solving the corresponding micro-scale problems.

In addition, only for the solid phase, we evaluate

– the homogenized elasticity tensor,
– the homogenized coefficient of thermal expansion and
– the homogenized heat transfer coefficient k_S^{H} in (32).

(2) Solve the macroscopic heat conduction problem of the fluid phase for its macroscopic temperature distribution.
(3) Solve the macroscopic heat conduction problem of the solid phase for its macroscopic temperature distribution. Here, the heat transferred from the fluid phase is brought into the solid phase as a kind of heat source/sink according to the current temperature value, which may varies in space according to the solution obtained in Step (2).
(4) Using the macroscopic temperature distribution in the solid phase evaluated in Step (3), calculate the macroscopic strain and stress due to the macroscopic thermal expansion/contraction.
(5) Solve the macroscopic deformation problem along with the macroscopic "initial stress" evaluated in Step (4).
(6) Set the time step forward and go back to Step (2).

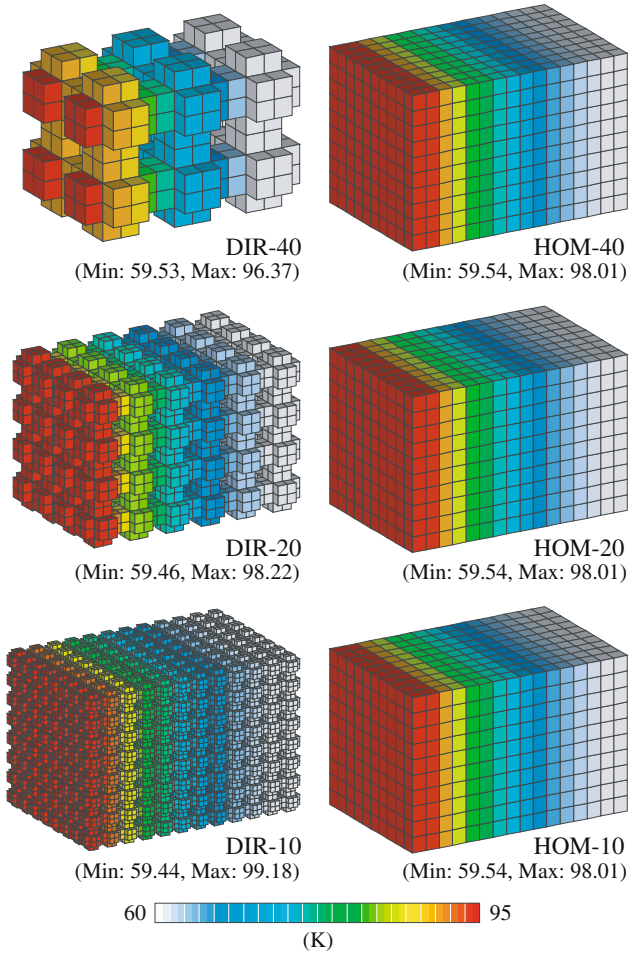

Fig. 9 Comparison of temperature-change distributions in fluid phase (time step: 50/100)

4.3 Numerical verification

We here present the results of the two-scale analyses to verify the validity and effectiveness of the proposed two-scale thermo-mechanical model in comparison with those of the direct analyses. In particular, our attention in this verification is drawn to the reproducibility of the effect of heat transfer at the pore surfaces in performing the two-scale thermo-mechanical coupling analyses. The relevance of the adopted solution method explained above is also examined during the course of the verification.

First, the heat conduction analyses for the fluid phase are carried out, and the temperature distributions at time step 50/100 are shown in Fig. 9. As can be seen form this figure, the temperature distributions obtained by the two-scale analyses are the same for the three models, HOM-40, HOM-20 and HOM-10. This makes sense since there is no factor to bring the scale effect on the heat conduction in the fluid phase. That is, the possibility of the heat transfer from the solid phase to the fluid phase has been excluded, and the homogenized heat conduction coefficients calculated with three separate unit cells of the same volume fraction of pores must be the same in theory. For reference, the temperature distributions in the fluid phase are very similar to those of the two-scale analyses, and appear to exhibit convergence trends.

As appeared in the last term of the governing equation (43) for the solid phase, the proposed two-scale model has a heat source/sink-like effect due to the "internal" heat transfer, the amount of which is proportional to the difference in temperature between the solid and fluid phases at the pore surfaces $T^0 - \hat{T}_S$. The constant of proportionality is the homogenized coefficient k_S^{H} that causes the scale effect as demonstrated earlier with Fig. 3. Here, the temperature distribution obtained for the fluid phase can be regarded as the data distribution of $\hat{T}_S$ for the solid phase. With this one and only heat supply, the temperature distributions in the solid phase at time step 50/100 can be obtained for the three separate cases, as shown in Fig. 10 along with those of the direct analyses. As can be seen from the figure, the temperature distributions in HOM-40, HOM-20 and HOM-10 are all different, with each of them resembling the result of the corresponding direct analysis. More specifically, the smaller the pore size, the higher the maximum and the minimum temperature values

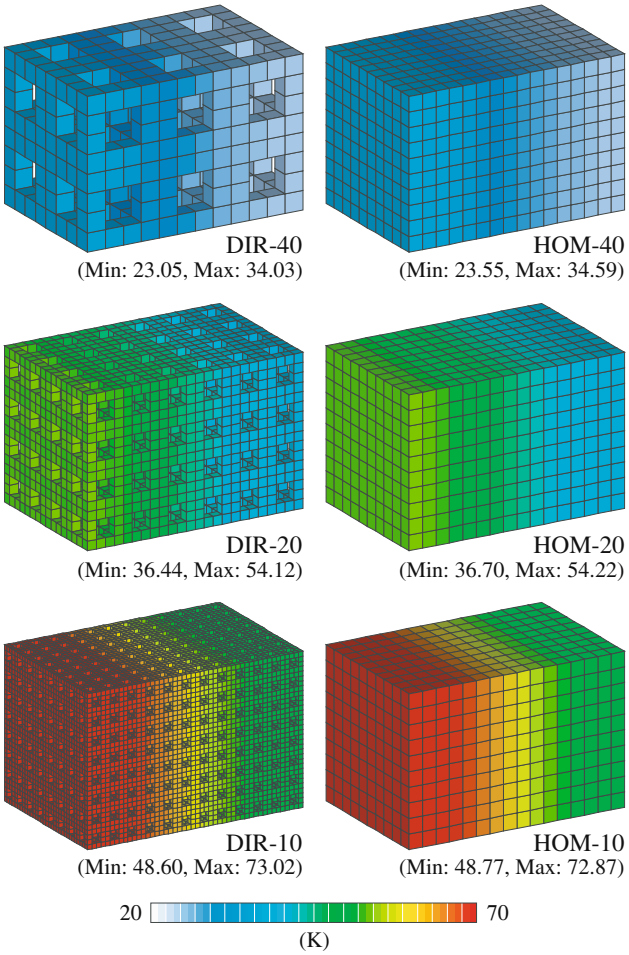

Fig. 10 Comparison of temperature-change distributions in solid phase (time step: 50/100)

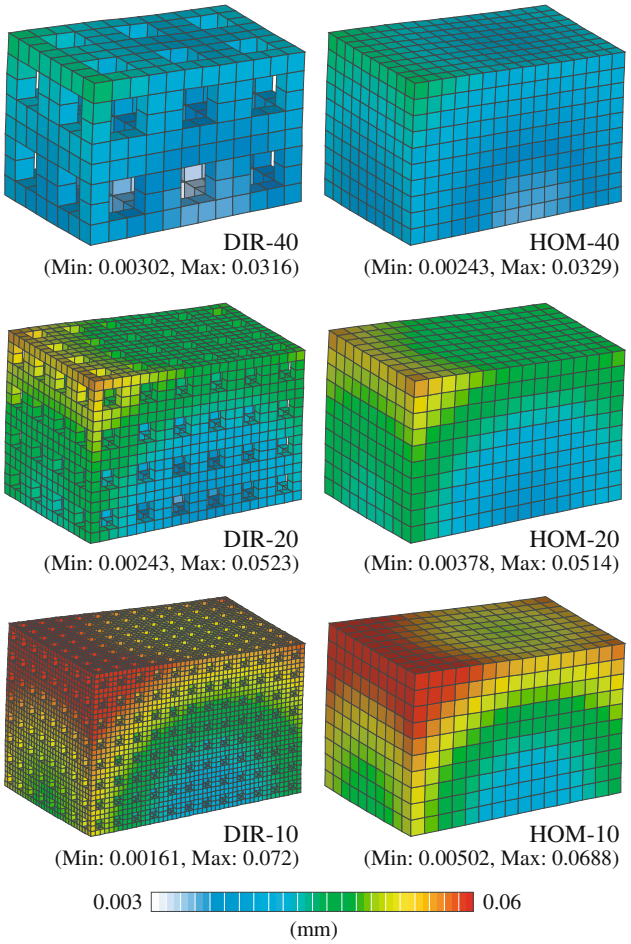

Fig. 11 Comparison of displacement-norm distributions in solid phase (time step: 50/100)

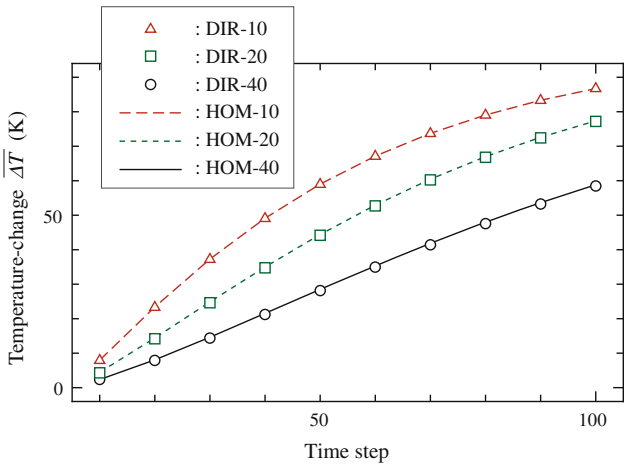

Fig. 12 Comparison of time histories of temperature-change in surface C of solid phase

in the solid phase. This is because the constant of proportionality k_S^{H}, which reflects the ratio of the pore surface area to the unit cell volume, increases, as the pore size, namely L_{RVE}, becomes smaller. The results verify the validity and relevance of the present two-scale model, which involves the effect of internal heat transfer.

Once the temperature distribution in the solid phase is obtained, it can be used as a datum for the macroscopic equilibrium problem of the solid phase subjected to the thermal expansion/contraction. Figure 11 shows the comparison of the macroscopic deformation patterns of the solid phase. Here, the L_2 norm $\|\boldsymbol{u}\|$ is employed for the contour plots. As can be seen from the figure, the patterns in HOM-40, HOM-20 and HOM-10, each of which reflects the corresponding temperature distribution in Fig. 10, are consistent with those of DIR-40, DIR-20 and DIR-10, respectively.

Figures 12 and 13, respectively show the changes in the time of the temperature and the displacement values over the internal surface C as defined in Fig. 4, which is perpendicular to the x_1-axis and located at $x_1 = 60$ mm. The vertical axes in the figures are computed by the following evaluation formulae:

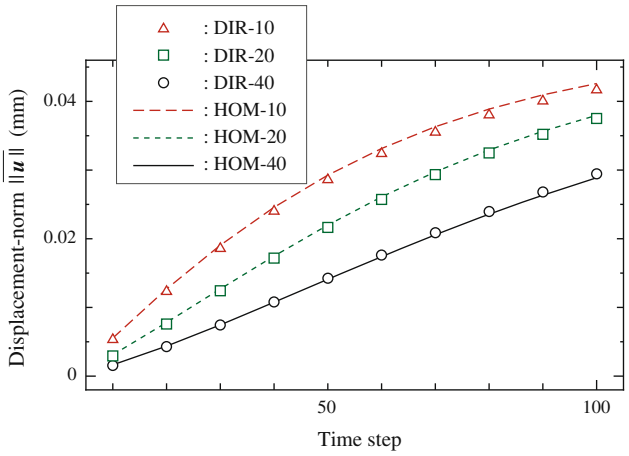

Fig. 13 Comparison of time histories of displacement-norm in surface C of solid phase

$$\overline{\theta^0} = \frac{\left(\int_{\Gamma_C} (\theta^0)^2 \, d\Gamma\right)^{1/2}}{\int_{\Gamma_C} d\Gamma}, \quad \overline{\|\boldsymbol{u}\|} = \frac{\left(\int_{\Gamma_C} \boldsymbol{u} \cdot \boldsymbol{u} \, d\Gamma\right)^{1/2}}{\int_{\Gamma_C} d\Gamma} \tag{79}$$

where Γ_C indicates the internal surface C. It can be found that the macroscopic response obtained by the two-scale analyses agree with those of the direct analyses quantitatively, even though the unit cell sizes for the direct analyses are finite. Also, these figures clearly illustrate the scale effect involved in the proposed two-scale thermo-mechanical model derived by the mathematical theory of homogenization. That is, a larger amount of heat can be transferred from the fluid phase to the solid phase as the proportion of the pore surfaces area to the unit cell volume increases.

As in single-physics computational homogenization, it is possible to evaluate the actual micro-scale thermo-mechanical responses of a unit cell located *at* any macroscopic point, if necessary. The numerical analysis for this process is called 'localization' and, in linear problems like the ones in this investigation, it can be done with the characteristic functions associated with the macroscopic temperature gradients for the heat conduction problem or the macroscopic strain for the deformation problem; that is, Eqs. (54) and (77) are utilized. Figure 15 shows the micro-scale temperature distributions as well as the micro-scale deformed configurations of unit cells located at separate macro-scale points along with the corresponding macro-scale responses at time step 10/100.

Finally, Fig. 14 shows the computation times spent for the direct and two-scale analyses. In this study, we utilized a standard personal computer with the CPU of intel Xeon X5260 with clock frequency 3.33 GHz and the intel FORTRAN compiler on a Windows OS. Needless to say, a direct analysis requires a large amount of time, which increases exponentially the smaller the size of the unit cell. On the contrary, the computation time required for the two-scale analyses is much less expensive than that of the direct analyses and never changes. The superiority of the proposed two-scale model over the full-scale model associated with direct analyses is obvious.

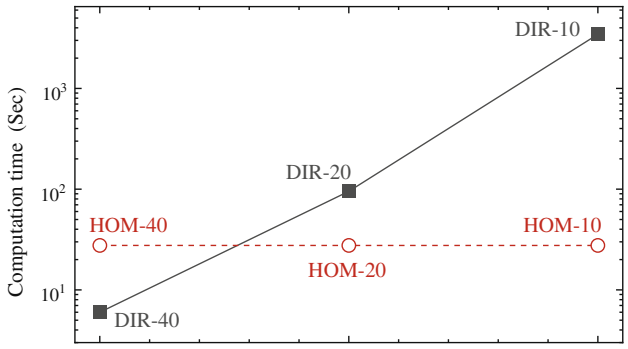

Fig. 14 Comparison of computation-time

5 Concluding remarks

A two-scale thermo-mechanical coupled model for porous solids has been proposed. The model was derived by applying the homogenization method, which extensively utilizes the method of asymptotic expansions, and enables us to take into account the heat transfer at pore surfaces. This model was implemented into our own two-scale analysis code, which is based on the weak coupling method to deal with the coupling between heat conduction and deformation problems. The validity of this two-scale model and the effectiveness of the developed two-scale analysis method have been verified by making comparison with the single-scale direct analyses. During the course of this numerical verification, it was well demonstrated that the proposed model is capable of reproducing the scale effect of heat exchange behavior between a porous solid and fluid filling pores.

As anticipated in the numerical verification, one of the straightforward application of the present framework is the coupling with fluid flow in porous media. That is, the heat is not only conducted in the fluid phase, but also transported by fluid advection when a heated or cooled fluid flows into a channel made of small pores.

Since neither geometrical nor material nonlinearities were considered in this study, the method of two-scale analysis becomes, consequently, very simple. In fact, all the macroscopic material behaviors is determined prior to the macroscopic analyses. That is, the homogenized material properties can be evaluated either by the geometrical information of microstructures or by the characteristic functions, which are obtained from micro-scale problems.

However, once some sort of nonlinearities have to be taken into account, the macroscopic mechanical behavior becomes a function of the macroscopic deformation and the

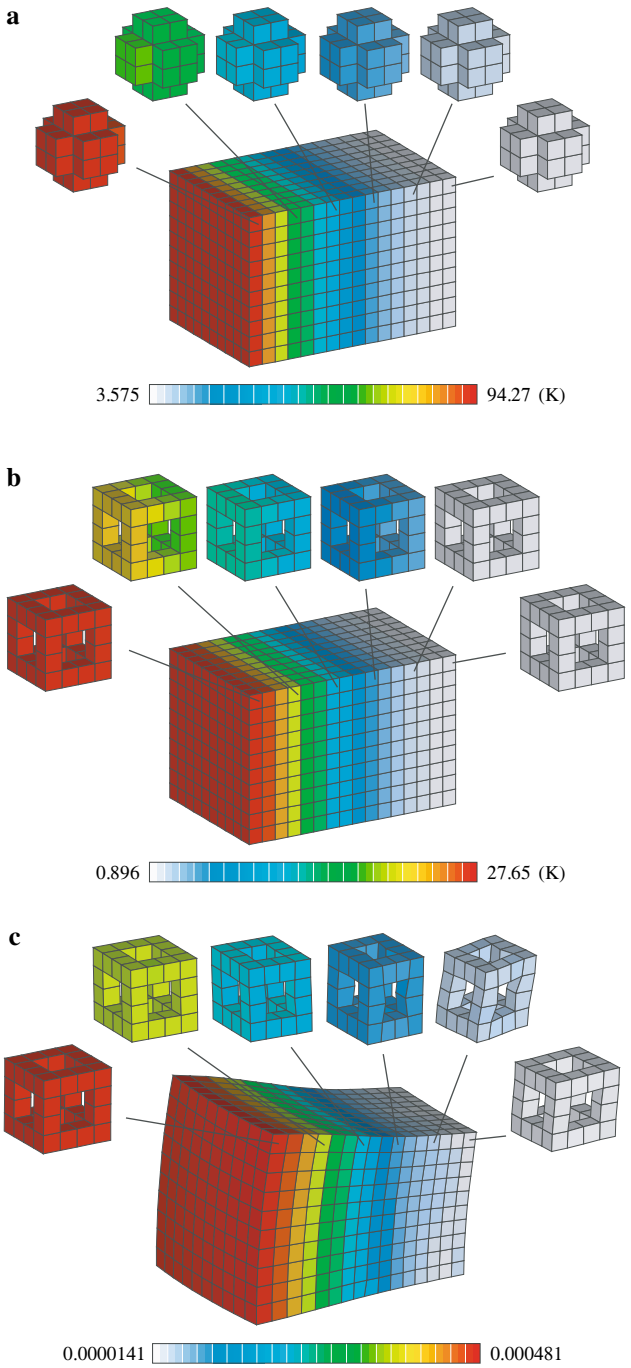

Fig. 15 Micro and macroscopic results in multi-scale analysis HOM-10 (time step: 10/100): **a** temperature-change in fluid phase; **b** temperature-change in solid phase; **c** strain norm in solid phase

macroscopic thermal behavior becomes a function of the macroscopic heat. This means that microscopic problems have to be solved for all the microscopic thermo-mechanical behaviors associated with macroscopic material points at all the time steps. Since solution strategies for such nonlinear two-scale problems have been established as in [22,23,16], the extension of the present framework to nonlinear problems is relatively easy, though realized at a high computational cost. In this context, the present formulation can be applied to the two-scale nonlinear analysis for material deterioration involving micro-cracks caused by thermal or chemical attack. This is currently being prepared.

Acknowledgments It is our pleasure to dedicate the manuscript to the memory of Professor Hirohisa Noguchi, affectionately known as Hiro, who was a close colleague of the authors. Fortunately, the authors had many chances to discuss numerical methods for multi-scale and multi-physics analysis like the present one with Hiro over the years. The authors appreciate the intellectual stimulation that he provided and gradually value his contributions to our work and lives.

References

1. Bear J (1988) Dynamics of fluids in porous media. Dover, New York
2. Mezedur M, Kaviany M, Moore W (2004) Effect of pore structure, randomness and size on effective mass diffusivity. AIChE J 48:15–24
3. Jen TC, Yan TZ (2005) Developing fluid flow and heat transfer in a channel partially filled with porous medium. Int J Heat Mass Transf 48:3995–4009
4. Xu RN, Jiang PX (2008) Numerical simulation of fluid flow in microporous media. Int J Heat Fluid Flow 29:1447–1455
5. Benssousan A, Lions JL, Papanicoulau G (1978) Asymptotic analysis for periodic structures. North-Holland, Amsterdam
6. Sanchez-Palencia E (1980) Non-homogeneous media and vibration theory. Lecture note in physics, vol 127. Springer, Berlin
7. Devries F, Dumontet H, Duvaut G, Léné F (1989) Homogenization and damage for composite structures. Int J Num Meth Eng 27:285–298
8. Guedes JM, Kikuchi N (1990) Preprocessing and postprocessing for materials based on the homogenization method with adaptive finite element method. Comput Methods Appl Mech Eng 83:143–198
9. Golanski D, Terada K, Kikuchi N (1997) Macro and micro scale modeling of thermal residual stresses in metal matrix composite surface layers by the homogenization method. Comput Mech 19:188–202
10. Terada K, Ito T, Kikuchi N (1998) Characterization of the mechanical behaviors of solid-fluid mixture by the homogenization method. Comput Methods Appl Mech Eng 153:223–257
11. Chung PW, Tamma KK (2001) Homogenization of temperature-dependent thermal conductivity in composite materials. AIAA J Thermophys Heat Transf 15:10–17
12. Laschet G (2002) Homogenization of the thermal properties of transpiration cooled multi-layer plates. Comput Methods Appl Mech Eng 191:4535–4554
13. Kamiński M (2003) Homogenization of transient heat transfer problems for some composite materials. Int J Eng Sci 41:1–29
14. Özdemir I, Brekelmans WAM, Geers MGD (2008) Computational homogenization for heat conduction in heterogeneous solids. Int J Num Meth Eng 73:185–204
15. Zhang HW, Zhang S, Bi JY, Schrefler BA (2007) Thermo-mechanical analysis of periodic multiphase materials by a multiscale asymptotic homogenization approach. Int J Num Meth Eng 69:87–113
16. Özdemir I, Brekelmans WAM, Geers MGD (2008) FE^2 computational homogenization for the thermo-mechanical analysis of heterogeneous solids. Comput Methods Appl Mech Eng 198:602–613

17. Terada K, Kikuchi N (2003) Introduction to the method of homogenization. The JSCES lecture note series I, Maruzen, Tokyo (in Japanese)
18. Hornung U (1991) Homogenization and porous media. Springer, New York
19. Yu Q, Fish J (2002) Multiscale asymptotic homogenization for multiphysics problems with multiple spatial and temporal scales: a coupled thermo-viscoelastic example problem. Int J Solids Struct 39:6429–6452
20. Zhang H, Zhang S, Gui X, Bi J (2005) Multiple spatial and temporal scales method for numerical simulation of non-classical heat conduction problems: one dimensional case. Int J Solids Struct 42:877–899
21. Auriault JL (1983) Effective macroscopic description of heat conduction in periodic composites. Int J Heat Mass Transf 26:861–869
22. Terada K, Kikuchi N (1995) Nonlinear homogenization method for practical applications. In: Ghosh S, Ostoja-Starzewski M (eds) Computational methods in micromechanics. AMD, vol 212/MD, vol 62. AMSE, New York, pp 1–16
23. Terada K, Kikuchi N (2001) A class of general algorithms for multi-scale analyses of heterogeneous media. Comput Methods Appl Mech Eng 190:5427–5464